Pump-Probe Anisotropies of Fenna-Matthews-Olson Protein Trimers from *Chlorobium tepidum*: A Diagnostic for Exciton Localization?

Sergei Savikhin, Daniel R. Buck, and Walter S. Struve
Ames Laboratory, U.S. Department of Energy, and Department of Chemistry, Iowa State University, Ames, Iowa 50011 USA

ABSTRACT Exciton calculations on symmetric and asymmetric Fenna-Matthews-Olson (FMO) trimers, combined with absorption difference anisotropy measurements on FMO trimers from the green bacterium *Chlorobium tepidum*, suggest that real samples exhibit sufficient diagonal energy disorder so that their laser-excited exciton states are noticeably localized. Our observed anisotropies are clearly inconsistent with 21-pigment exciton simulations based on a threefold-symmetric FMO protein. They are more consistent with a 7-pigment model that assumes that the laser-prepared states are localized within a subunit of the trimer. Differential diagonal energy shifts of 50 cm^{-1} between symmetry-related pigments in different subunits are large enough to cause sharp localization in the stationary states; these shifts are commensurate with the ~95 cm^{-1} inhomogeneous linewidth of the lowest exciton levels. Experimental anisotropies (and by implication steady-state linear and circular dichroism) likely arise from statistical averaging over states with widely contrasting values of these observables, in consequence of their sensitivity to diagonal energy disorder.

INTRODUCTION

The Fenna-Matthews-Olson bacteriochlorophyll (BChl) *a*-protein complex is involved in electronic energy transfers from peripheral light-harvesting antennas (chlorosomes) to reaction centers in green photosynthetic bacteria (Olson, 1980a). It has been much studied (Blankenship et al., 1995), because its three-dimensional structure was the first one reported for any photosynthetic pigment-protein complex (Matthews and Fenna, 1980; Tronrud et al., 1986). This water-soluble protein contains three identical polypeptide subunits, organized about a threefold proper rotation axis. Each subunit is a folded β-sheet, the hydrophobic interior of which encloses seven BChl *a* pigments with well defined positions and orientations. The low-temperature Q_y absorption spectrum of Fenna-Matthews-Olson (FMO) trimers (unlike the featureless Q_y spectra of the LH1 and LH2 BChl *a*-protein antennnas of purple bacteria; cf. Zuber and Cogdell, 1995; Sundström and van Grondelle, 1995) exhibits considerable structure, with band maxima near 825, 815, and 805 nm as well as several shoulders (Philipson and Sauer, 1972; Olson et al., 1976). Exciton modeling studies (Lu and Pearlstein, 1993; Pearlstein, 1992) of the Q_y absorption and circular dichroism (CD) spectra of FMO trimers from the green bacterium *Prosthecochloris aestuarii* (Philipson and Sauer, 1972; Olson et al., 1976), together with spectral hole-burning experiments on the FMO proteins from *P. aestuarii* and *Chlorobium tepidum* (Johnson and Small, 1991; Reddy et al., 1995) indicate the presence of strong resonance couplings (up to ~200 cm^{-1}) between BChl *a* pigments within the same protein subunit. The couplings between pigments belonging to different subunits of a trimer are substantially weaker ($\leq$16 cm^{-1}; Pearlstein, 1992). Owing to this hierarchy between intra- and intersubunit couplings, the latter have a relatively minor influence on the isotropic Q_y absorption spectrum. Each of the seven Q_y exciton components arising from pigments within a single subunit becomes split into a nondegenerate level and a doubly degenerate pair of levels. These splittings are in the low tens of cm^{-1}. By contrast, the seven exciton components for an isolated FMO subunit are dispersed over some 750 cm^{-1}, from ~780 to 825 nm.

Although the intersubunit couplings can be viewed as perturbations to the isotropic absorption spectrum, they profoundly affect the CD spectrum. In model calculations limited to one subunit, parametric searches of the seven unknown BChl *a* diagonal energies could not yield simultaneous fits to experimental absorption and CD spectra of FMO trimers from *P. aestuarii*. However, successful fits to both spectra were achieved in calculations extending over the whole trimer (Pearlstein, 1992).

We recently reported an optical pump-probe study of exciton level relaxation in FMO trimers from *Cb. tepidum* at 19 K (Buck et al, 1997). At this temperature, the absorption difference spectra (like the steady-state absorption spectrum) are highly structured and undergo complex spectral evolution. Global analysis of ΔA spectra obtained by exciting the trimers at 789 nm (near the blue edge of the Q_y spectrum) yielded a kinetic model for interlevel relaxation, with lifetimes ranging from 170 fs to 11 ps. (The corresponding spectral equilibration becomes greatly accelerated at higher temperature. It is essentially complete within several hundred femtoseconds at 300 K (Savikhin et al., 1994a; Savikhin and Struve, 1994).) These absorption difference spectra were compared with ΔA spectral simulations, which included contributions from photobleaching (PB) of ground $\rightarrow$ one-exciton transitions, stimulated emission (SE), and excited state absorption (ESA) arising from one-exciton $\rightarrow$

Received for publication 21 April 1997 and in final form 1 July 1997.
Address reprint requests to Dr. Walter S. Struve, Department of Chemistry, Iowa State University, Gilman Hall, Ames, IA 50011-3111. Tel.: 515-294-4276; Fax: 515-294-1699; E-mail: wstruve@ameslab.gov.

0006-3495/97/10/2090/07 $2.00

two-exciton transitions. These simulations incorporated BChl *a*-BChl *a* resonance interactions computed by Pearlstein (1992) using the point monopole method with BChl *a* Q_y transition charge distribution from Weiss (1972). The BChl *a* diagonal energies were derived by Lu and Pearlstein (1993) from best fits of their simulated absorption and CD spectra to the spectra of Olson et al. (1976; hereafter called OKT) or the spectra of Philipson and Sauer (1972; hereafter called PS). By combining our global analysis with single-level ΔA spectra computed from the OKT diagonal energies, we were able to qualitatively reproduce the main features of the experimental ΔA spectral evolution. Considerably less satisfactory agreement was achieved in simulations using the PS diagonal energies. We briefly addressed whether our isotropic ΔA spectra could be used to differentiate between excitations that remained delocalized over the entire trimer during the time window of 0–11 ps at 19 K and excitations that had become confined to one subunit. The differences between isotropic ΔA spectra simulated using the 7- and 21-pigment exciton models proved to be subtle (and smaller than experimental uncertainty). This outcome was traceable to the order-of-magnitude disparity between the dominant intersubunit interactions on the one hand and the intrasubunit interactions plus site energy differences between BChl pigments within a subunit on the other.

Optical anisotropies are apt to be far more sensitive to localization in FMO trimers. Although the transition moments for the seven exciton components for an isolated (asymmetric) subunit of an FMO trimer have irregular orientations, by symmetry, each of the 21 transitions to one-exciton levels in the trimer is either *z* polarized (nondegenerate) or *xy* polarized (doubly degenerate). The *z* axis is defined as the C_3 proper rotation axis. Hence, anisotropies (unlike isotropic ΔA spectra) may be drastically influenced by the extent of exciton localization. This expectation is borne out in this paper by anisotropy simulations for FMO trimers at various pump-probe wavelength combinations and exciton domain sizes. These simulations are compared with experimental one- and two-color anisotropies for FMO trimers from *Cb. tepidum* at 19 K.

MATERIALS AND METHODS

FMO trimers were isolated from *Cb. tepidum* according to the method of Olson (1980b), with the modifications described by Savikhin et al. (1994a). The room temperature absorption spectrum, which resembles that of FMO trimers isolated from other green photosynthetic bacteria (Blankenship et al., 1993), exhibits maxima at 809, 602, 371, and 262 nm. The present experiments were performed at 19 K, to resolve features in the Q_y spectrum arising from well defined groups of exciton transitions. The self-mode-locked Ti:sapphire laser and pump-probe optics have been described elsewhere (Savikhin et al., 1994b). In our radiofrequency (RF) multiple modulation system, the probe beam-detecting photodiode was incorporated into an RLC input loop tuned to the RF detection frequency (Savikhin, 1995). Samples were housed between quartz and sapphire optical flats in thermal contact with the end of a Cu cold finger in an Air Products (Allentown, PA) DE202 closed-cycle He expander module. The sapphire window provided thermal conductivity for cooling, whereas the polarized light beams traversed the low-birefringence quartz window before entering the sample.

Anisotropies $r(t)$ were computed from the polarized absorption difference profiles $\Delta A_{\parallel}(t)$, $\Delta A_{\perp}(t)$ via

$$r(t) = [\Delta A_{\parallel}(t) - \Delta A_{\perp}(t)]/[\Delta A_{\parallel}(t) + 2\Delta A_{\perp}(t)] \quad (1)$$

In one-color experiments, the laser pulse spectrum was shaped using an intracavity birefringence filter, yielding output pulses with ~10-nm full width at half maximum (fwhm) and ~150-fs autocorrelation function width. For two-color experiments, the full Ti:laser output bandwidth was used (up to ~40 nm), corresponding to a ~70-fs autocorrelation width. The pump and probe spectra were then selected using bandpass interference filters (CVI Corp., Albuquerque, NM); the transmitted bandwidth was typically ~7 nm. The instrument function in two-color experiments showed ~200-fs cross-correlation, due to dispersion in the interference filters. The laser spectra incident at the sample were measured during experiments using a Czerny-Turner monochromator (7.9 nm/mm dispersion), with its output imaged onto the linear CCD array of a Unidata BP2048 beam profiler.

According to OKT simulations of the absorption and CD spectra for FMO trimers from *P. aestuarii,* the three lowest-energy exciton transitions prepare states near 825 nm (dominated by excitations on pigments 6 and 7 in the numbering scheme of Matthews and Fenna, 1980). The next six transitions excite two groups of three levels each, clustered near 815 nm. These levels are dominated by excitations on pigments 3–6 (Pearlstein, 1992; Lu and Pearlstein, 1993; Buck et al., 1997). The corresponding long-wavelength absorption bands for FMO trimers from *Cb. tepidum* occur at essentially the same wavelengths as those for *P. aestuarii* but with different intensities. The differences likely arise from minor variations in the pigment positions and orientations between the two species, as their FMO proteins are 78% homologous and all of the pigment-coordinating residues are conserved (Daurrat-Larroque et al., 1986). The pump and probe pulse spectra for the present experiments and simulations were each centered near one of these groups of transitions (i.e., near 815 or 825 nm), without significantly overlapping the other group. This avoids the appearance of strong oscillations in $r(t)$, which occur at low temperatures in FMO trimers from *Cb. tepidum* when the pump and probe spectra straddle both groups of transitions (S. Savikhin, D. R. Buck, and W. S. Struve, submitted for publication). These oscillations (which are dominated by a component with a ~220-fs period) do not arise from coherent nuclear motion but from quantum beating between contrastingly polarized transitions to the respective level groups. The origin of these oscillations are being treated in depth in a separate paper, and they are not considered here.

THEORY

The anisotropy calculations are a straightforward extension of the theory for isotropic absorption difference spectra in FMO trimers, which has recently been described (Buck et al., 1997). An antenna containing N strongly coupled pigments exhibits N one-exciton states $|\psi_i^{(1)}\rangle$, which may be expanded in terms of the basis functions $|\chi_j^{(1)}\rangle$ that localize Q_y excitation on pigments j ($j = 1, \ldots, N$) as

$$|\psi_i^{(1)}\rangle = \sum_{j=1}^{N} c_j^i |\chi_j^{(1)}\rangle \quad (2)$$

The one-exciton level energies $E_i^{(1)}$ and expansion coefficients c_j^i are obtained by diagonalizing the Hamiltonian in this basis and are necessary for evaluating the contributions of PB and SE to the absorption difference spectrum. The $N(N-1)/2$ two-exciton states

$$|\psi_k^{(2)}\rangle = \sum_{ij} d_{ij}^{(k)} |\chi_{ij}^{(2)}\rangle \quad (3)$$

can be expanded in terms of the $N(N-1)/2$ doubly excited basis functions $|\chi_{ij}^{(2)}\rangle$, which describe Q_y excitations of pigment pairs (ij). The two-exciton levels $E_k^{(2)}$ and expansion coefficients $d_{ij}^{(2)}$ are generated by diagonalizing the Hamiltonian in the doubly excited basis. They influence the ESA spectrum that arises from one-exciton → two-exciton transitions. The contribution to the ΔA signal arising from photobleaching of the transition to one-exciton state $|\psi_{i'}^{(1)}\rangle$, after laser excitation of one-exciton state $|\psi_i^{(1)}\rangle$, is proportional to

$$PB = -|\vec{E}_u(\lambda_{0i}) \cdot \langle 0|\vec{\mu}|\psi_i^{(1)}\rangle|^2 |\vec{E}_r(\lambda_{0i'}) \cdot \langle \psi_{i'}^{(1)}|\vec{\mu}|0\rangle|^2$$
$$= -|\sum_j c_j^i \vec{E}_u(\lambda_{0i}) \cdot \langle 0|\vec{\mu}|\chi_j^{(1)}\rangle|^2 |\sum_{j'} c_{j'}^{i'} \vec{E}_r(\lambda_{0i'}) \cdot \langle \chi_{j'}^{(1)}|\vec{\mu}|0\rangle|^2 \quad (4)$$

Here $|0\rangle$ is the N-pigment electronic ground state, $\vec{E}_u(\lambda_{0i})$, $\vec{E}_r(\lambda_{0i'})$ are the pump and probe electric fields at the transition wavelengths λ_{0i}, $\lambda_{0i'}$, and μ is the electric dipole moment operator. According to Eq. 4, excitation of any one-exciton level bleaches the entire one-exciton spectrum uniformly. The corresponding probability of stimulated emission from one-exciton state $|\psi_{i'}^{(1)}\rangle$ depends on the fractional population $P_{i'}$ in that level,

$$SE = -P_{i'}|\vec{E}_u(\lambda_{0i}) \cdot \langle 0|\vec{\mu}|\psi_i^{(1)}\rangle|^2 |\vec{E}_r(\lambda_{0i'}) \cdot \langle \psi_{i'}^{(1)}|\vec{\mu}|0\rangle|^2$$
$$= -P_{i'}|\sum_j c_j^i \vec{E}_u(\lambda_{0i}) \cdot \langle 0|\vec{\mu}|\chi_j^{(1)}\rangle|^2 |\sum_{j'} c_{j'}^{i'} \vec{E}_r(\lambda_{0i'}) \cdot \langle \chi_{j'}^{(1)}|\vec{\mu}|0\rangle|^2 \quad (5)$$

This implicitly assumes that the Stokes shifts between PB and SE are negligible; significant Stokes shifts (relative to the exciton component bandwidths, see below) have not been detected in fluorescence studies of FMO trimers and are not expected for BChl *a* pigments in the hydrophobic protein interior. The ESA signal arising from the one-exciton → two-exciton transition $|\psi_{i'}^{(1)}\rangle \rightarrow |\psi_k^{(2)}\rangle$ after excitation of state $|\psi_i^{(1)}\rangle$ is

$$ESA = P_{i'}|\vec{E}_u(\lambda_{0i}) \cdot \langle 0|\vec{\mu}|\psi_i^{(1)}\rangle|^2 |\vec{E}_r(\lambda_{i'k}) \cdot \langle \psi_{i'}^{(1)}|\vec{\mu}|\psi_k\rangle|^2 \quad (6)$$

$$= P_{i'}|\sum_j c_j^i \vec{E}_u(\lambda_{0i}) \cdot \langle 0|\vec{\mu}|\chi_j^{(1)}\rangle|^2 |\sum_{j'} c_{j'}^{i'} d_{mn}^k \vec{E}_r(\lambda_{i'k}) \cdot \langle \chi_{j'}^{(1)}|\vec{\mu}|\chi_{mn}^{(2)}\rangle|^2$$

In each of Eqs. 4–6, the parallel and perpendicular components of the absorption difference signal are computed using $\vec{E}_r \parallel \vec{E}_u$ and $\vec{E}_r \perp \vec{E}_u$, respectively. The signals are averaged over the random orientations of FMO trimers, over the laser pump and probe spectra, and over the finite spectral widths of the exciton components. Lu and Pearlstein (1993) simulated the OKT absorption and CD spectra of FMO trimers from *P. aestuarii* by assigning 95–342 cm^{-1} widths to symmetric Gaussian one-exciton components; in this work, we arbitrarily use 150 cm^{-1} fwhm symmetric Gaussians for each of the ground → one-exciton and one-exciton → two-exciton transitions (Buck et al., 1997). The anisotropies are then computed from Eq. 1, using $\Delta A_{\parallel(\perp)} = ESA_{\parallel(\perp)} + PB_{\parallel(\perp)} + SE_{\parallel(\perp)}$.

Fig. 1 shows one-color FMO anisotropies for wavelengths between 770 and 830 nm, simulated for 150 cm^{-1} (~10 nm) bandwidth laser pulses. These are prompt anisotropies, evaluated under the assumption that negligible level relaxation has occurred before probing. Our calculations do not include optical coherences, which would need to be considered during the time regime of pump-probe overlap (Chachisvilis and Sundström, 1996). The curves labeled trimer and monomer are anisotropies simulated using 21- and 7-pigment exciton models, respectively. The latter model is generated by limiting the basis sets to excitations on pigments 1–7 and excluding those from pigments 8–21. The resonance couplings are taken from Pearlstein (1992), and the diagonal energies are the ones obtained from fits (Lu and Pearlstein, 1993) to the OKT absorption and CD spectra. For most wavelengths, the monomer and trimer

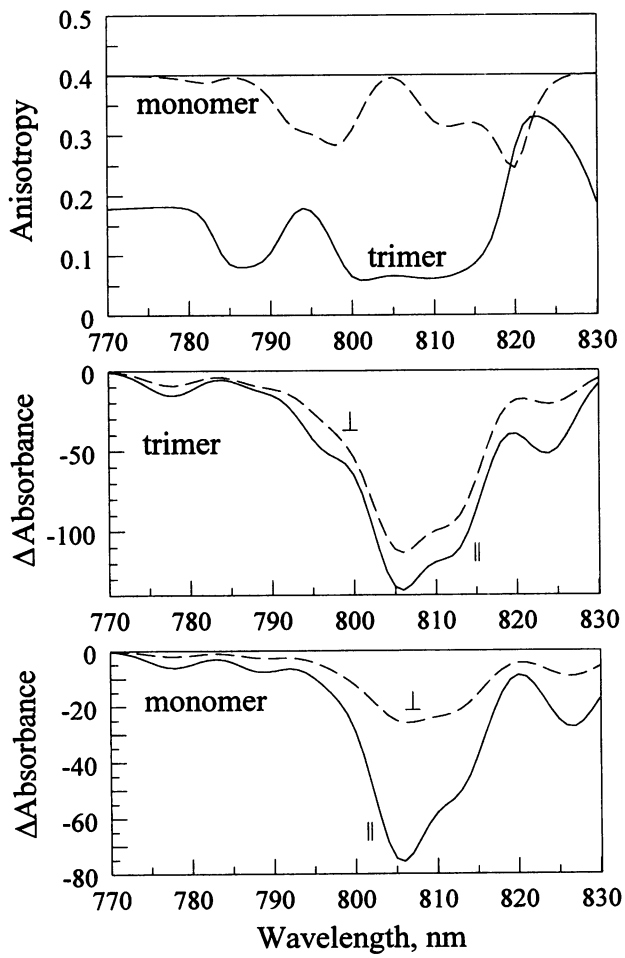

FIGURE 1 Simulated one-color anisotropies for FMO trimers from *P. aestuarii* versus pump-probe wavelength (*top panel*) and simulated parallel and perpendicular absorption difference signals for trimer and monomer models (*center* and *bottom panels*). Symbols ∥ and ⊥ denote parallel and perpendicular absorption difference signals. Laser pulses are 10 nm fwhm. Trimer and monomer curves are computed from 21- and 7-pigment exciton models, respectively. In Figs. 1–4, positive and negative ΔA values correspond to ESA and PB/SE.

models yield contrasting anisotropies; however, these one-color anisotropies are always bounded between 0 and 0.4.

Fig. 2 shows prompt two-color anisotropies, simulated for the pump wavelengths 815 and 825 nm as functions of the probe wavelength. The pump and probe spectral widths are 7 nm. As before, the monomer and trimer models often yield widely divergent anisotropies. A new feature here is the occurrence (for some probe wavelengths considerably removed from the pump wavelength) of "exotic" anisotropies with negative values as well as values >0.4. Such anisotropies occur for probe wavelengths where ESA transitions (with polarizations strongly skewed from those of the pumped transitions) contribute significantly to the total signal. They do not occur in the one-color anisotropies (Fig. 1), where the signal generally has large contributions from PB and SE transitions polarized parallel to the pumped transitions.

Experimental anisotropies

Fig. 3 shows polarized absorption difference signals and anisotropies for FMO trimers from *Cb. tepidum* excited at 19 K with 815-nm laser pulses and probed at either 815 or 825 nm. A dominant decay pathway from the six 815-nm levels populates the 825-nm level group with ~2.5 ps kinetics at this temperature (Buck et al., 1997). This time constant corresponds to the major PB/SE decay feature observed in the 815 → 815 nm profiles, and for most of the PB/SE rise behavior in the 815 → 825 nm profiles. The 815 nm one-color anisotropy stabilizes between 0.30 and 0.35 after pulse overlap and rises slightly during the next 2 ps. The 815 → 825 nm two-color anisotropy remains essentially constant at ~−0.12.

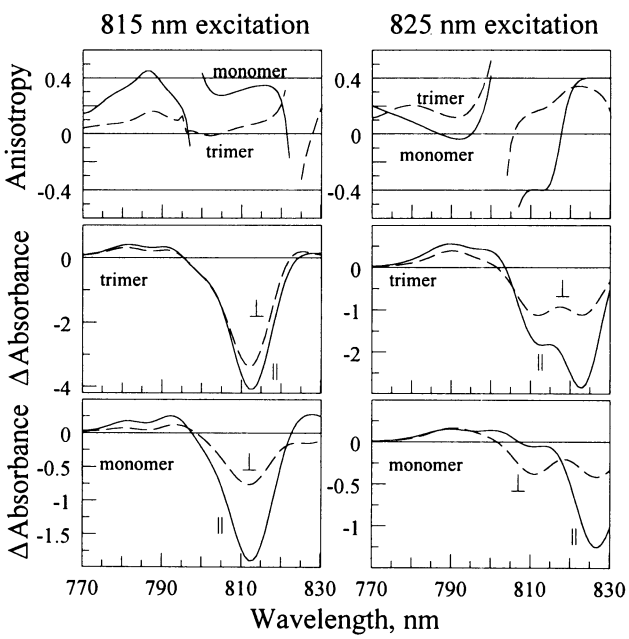

FIGURE 2 Simulated two-color anisotropies and polarized absorption difference spectra for FMO trimers from *P. aestuarii* as functions of probe wavelength, for pump wavelengths 815 nm (*left*) and 825 nm (*right*). Anisotropies are shown in top panels; absorption difference spectra for trimer and monomer models are shown in center and bottom panels, respectively. Laser pulses are 7 nm fwhm.

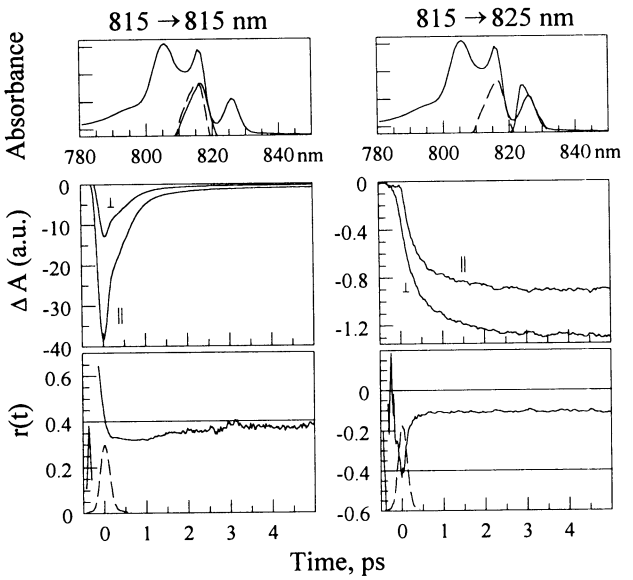

FIGURE 3 Experimental absorption difference profiles (*center*) and anisotropies (*bottom*) for FMO trimers from *Cb. tepidum* excited by 815-nm pulses at 19 K. The experiments are 815 → 815 nm (*left*) and 815 → 825 nm (*right*). Pump and probe pulse spectra (*dashed* and *solid curves*, respectively) are superimposed on the steady-state Q_y absorption spectrum in top panels. Dashed curves in the bottom panels are laser auto- or cross-correlations.

Fig. 4 shows the corresponding anisotropies obtained by exciting FMO trimers at 825 instead of 815 nm. The 825 → 815 nm anisotropy levels off near −0.30 shortly after pulse overlap. An anomaly in the parallel signal $\Delta A_{\parallel}$ for these wavelengths is a large, nominal PB/SE component with decay kinetics on a time scale commensurate with (but not identical to) the trailing edge of the pulse autocorrelation. There is no corresponding fast component in the perpendicular signal $\Delta A_{\perp}$. This may be a pseudo-two-color optical coherence of the type described by Chachisvilis and Sundström (1996). The 825 → 825 nm anisotropy appears to be ~0.25; the signal to noise is limited here by the small signals obtained in experiments at the red edge of the FMO Q_y spectrum, where the optical densities are low.

These experimental anisotropies all confirm the prediction in Figs. 1 and 2 that the one-color anisotropies of FMO trimers are bounded between 0 and 0.4, whereas two-color anisotropies can assume values outside this range. However, the measured anisotropies in Figs. 3 and 4 do not generally resemble the anisotropies simulated using the 21-pigment model. The prompt anisotropies computed using the 21-pigment model (Figs. 1 and 2) for the 815 → 815 and 825 → 815-nm experiments are +0.05 and +0.25, respectively. The corresponding empirical values (Figs. 3 and 4) are +0.35 and −0.30. Considerably better agreement is obtained using anisotropies computed from the 7-pigment

model (+0.37 and −0.40, respectively). The theoretical anisotropies for the 815 → 825 and 825 → 825 nm experiments yield little basis for differentiating between the two models. The probe wavelength variation of $r(0)$ for FMO trimers excited at 815 nm exhibits a singularity near 825 nm in both the 7- and 21-pigment models (Fig. 2), so that comparisons of the simulations with the 815 → 825 nm experiment are considerably less meaningful than for the other pump-probe wavelength combinations. (For that matter, neither model predicts that both $\Delta A_{\parallel}$ and $\Delta A_{\perp}$ will be dominated by PB/SE in this experiment, as is observed (Fig. 3). The total absorption difference signals are small in this region, and the neglect of BChl *a* monomer ESA (Becker et al., 1991) in the simulation may contribute disproportionately to the error at these wavelengths.) Both models predict similar $r(0)$ in the 825 → 825 nm experiment (0.40 and 0.35); the experimental value is 0.25. Although more wavelength combinations could have been investigated, our pump-probe experiments were limited to the long-wavelength 815 and 825 nm level groups, the decay kinetics of which are equal to or slower than 2.5 ps at 19 K (Buck et al., 1997). In this way, contributions of known level-to-level relaxation processes to experimental anisotropies were minimized during the subpicosecond time window.

DISCUSSION

The interpretation of our FMO anisotropy measurements is model dependent, because its reliability rests on a host of assumptions about the BChl resonance couplings and diagonal energies. The resonance couplings were derived from approximate pi electron wave functions for chlorophylls (Weiss, 1972), whereas the diagonal energies were obtained from parametric fits of theoretical absorption and CD spectra to experimental spectra (Pearlstein, 1992; Lu and Pearlstein, 1993). In our view, more accurate BChl resonance energies are needed, based on more realistic electronic wave functions, combined with analysis of medium effects on the couplings. Additional experimental constraints would better define the possible sets of BChl diagonal energies. Gülen (1996) has suggested that FMO linear dichroism and singlet-triplet absorption difference spectra would provide more incisive criteria for exciton modeling than absorption and CD spectra. Optimized fits to such spectra for FMO trimers from *P. aestuarii* were obtained when BChl 6 was assigned the lowest diagonal energy (Gülen, 1996); the lowest site energy belongs to BChl 7 in the OKT fits (Lu and Pearlstein, 1993). We have recently suggested that low-temperature time-resolved isotropic absorption difference spectra can furnish yet another criterion for exciton modeling (Buck et al., 1997). OKT simulations reproduce many of the features observed in ΔA spectra of FMO trimers from *Cb. tepidum* excited at 789 nm. Simulations based on the PS diagonal energies cannot (Buck et al., 1997), nor can simulations using Gülen's diagonal energies combined with the Pearlstein's (1992) resonance couplings (D. R. Buck, S. Savikhin, and W. S. Struve, unpublished work). In our experience, only the OKT simulations have consistently yielded reasonable fits to the absorption, CD, and absorption difference spectra. The resonance couplings used in all simulations to date have been computed from the crystal structure of FMO trimers from *P. aestuarii*, whereas our time-resolved ΔA and anisotropy experiments were done on FMO trimers from *Cb. tepidum*.

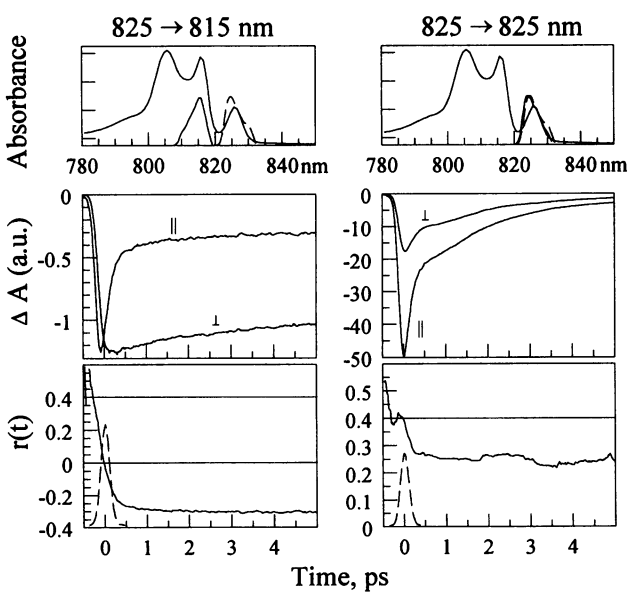

FIGURE 4 Experimental absorption difference profiles (*center*) and anisotropies (*bottom*) for FMO trimers from *Cb. tepidum* excited by 825-nm pulses at 19 K. The experiments are 825 → 815 nm (*left*) and 825 → 825 nm (*right*). Pump and probe pulse spectra (*dashed* and *solid curves*, respectively) are superimposed on the steady-state Q_y absorption spectrum in top panels. Dashed curves in the bottom panels are laser auto- or cross-correlations.

Given all of these caveats, our interpretations must be viewed as tentative rather than definitive. Several idealized scenarios can be envisaged for exciton state evolution during the first few hundred femtoseconds at 19 K.

First, the laser-prepared one-exciton levels are well described as threefold-symmetric, delocalized 21-pigment states, which can be modeled using suitable BChl site energies and resonance couplings (e.g., in the OKT simulation). This delocalization is fully maintained during the observation time window.

Second, FMO trimers in the low-temperature glass are distorted from C_3 symmetry to such an extent that the site energies for the corresponding pigments (e.g., BChls 7, 14, and 21) in different subunits are significantly dispersed (i.e., diagonal disorder). The laser-prepared states themselves may be well described by states similar to the ones considered in our 7-pigment anisotropy simulations; protein motions may cause farther localization.

Third, the laser excites 21-pigment states as in the first scenario, but random protein motions cause localization to smaller domain sizes during the time window, as is observed in J-aggregates (de Boer and Wiersma, 1990) and in

the LH2 antenna of purple photosynthetic bacteria (Pullerits and Sundström, 1996). A typical domain may comprise the seven BChl pigments within one subunit, but it may be larger or smaller. The domain size would likely depend on temperature (de Boer and Wiersma, 1990). The second and third scenarios differ in that the respective sources of exciton localization are static (diagonal disorder) and dynamic (protein motions). Combinations of these two scenarios are of course possible.

Our 21-pigment OKT simulations of the 815 → 815 and 825 → 815 nm anisotropies differ grossly from the measured anisotropies, and thus appear to rule out the first scenario. Indirect evidence already suggests that FMO excitations at measurable times are not delocalized over the entire trimer, because FMO trimers from *Cb. tepidum* at 300 K exhibit a 1.7–2 ps anisotropy component that appears to have no major counterpart in the one- or two-color isotropic absorption difference profiles. This component was assigned to equilibration among the lowest-energy Q_y states in the respective protein subunits. Similarly, the anisotropy decay components found at 19 K, which are considerably decelerated from those at 300 K (Savikhin and Struve, 1996), do not coincide with major isotropic decay-associated spectral components at that temperature (Buck et al., 1997).

The second scenario appears to be qualitatively consistent with our anisotropy data. The question arises as to whether a physically reasonable amount of energy disorder (which is bounded by the inhomogeneous broadening of the lowest-energy exciton components of FMO trimers) can cause significant localization in the laser-prepared stationary states. We investigated the sensitivity of the one-exciton wave functions to Hamiltonian symmetry-breaking, by altering the BChl diagonal energies in selected subunits without changing the resonance interactions. In the absence of symmetry breaking, the lowest-energy nondegenerate exciton component at 824 nm (in which the excitations are dominated by pigments 6 and 7 in the first subunit and by the equivalent pigments in the other subunits) exhibits one-third of the total excitation density (as computed from the sum of squares of expansion coefficients) in each of the three subunits. In the degenerate pair of states at 827 nm, the excitation density in each subunit (summed over those two states) is likewise one-third of the total. The excitations are thus fully delocalized among the subunits under C_3 symmetry.

Symmetry breaking was introduced by applying the diagonal energy shifts $+50$ cm^{-1} to each of the seven pigments in the first subunit, 0 cm^{-1} to the pigments in the second subunit, and -50 cm^{-1} to the pigments in the third. The twofold degeneracy in the 827-nm pair became lifted, yielding nondegenerate levels at 823, 827, and 830 nm. The corresponding one-exciton wave functions concentrated 86, 87, and 93% of their excitation densities in the first, second, and third subunits, respectively (principally on pigments 7, 14, and 21). Such strong localization in the stationary states is not surprising, as the largest interaction between pigments in neighboring subunits is only 16 cm^{-1}. These diagonal energy shifts of ± 50 cm^{-1} are commensurate with the spectral widths of the lowest three exciton components in the steady-state absorption spectrum, which Lu and Pearlstein (1993) modeled using 95 cm^{-1} symmetric Gaussian functions. These spectral widths are dominated by inhomogeneous broadening; the higher-energy exciton components exhibit considerable lifetime broadening as well (Johnson and Small, 1991). Excitation of such states in the distorted FMO trimer will produce anisotropies resembling the ones simulated above using the 7-pigment model. Realistically speaking, FMO trimers in a glass will exhibit a distribution of diagonal energy shifts between subunits and between pigments within a subunit. In the presence of this disorder, our calculations suggest that an experiment under 825-nm excitation will excite a distribution of physically distinct exciton states, ranging from highly symmetric states for trimers with essentially threefold symmetry to strongly localized states for diagonal energy shifts comparable to the inhomogeneous broadening profile fwhm. If the diagonal energies of pigments belonging to different subunits are uncorrelated, the statistics will be dominated by asymmetric trimers.

The localization was still pronounced when the site energies in the first and third subunits were shifted by $+30$ and -30 cm^{-1}; in this case, the resulting exciton components at 824, 827, and 829 nm concentrated 76, 74, and 87% of the excitation density in the first, second, and third subunits, respectively. Reducing the site energy shifts to ± 10 cm^{-1} yielded 825, 827, and 828 nm levels that concentrated 50, 48, and 74% of the excitation density in the respective subunits. Even for 10 cm^{-1} inhomogeneous broadening, the effects of localization are difficult to ignore.

Such symmetry breaking has major consequences for exciton simulations of FMO electronic structure. Diagonal disorder of only a few tens of cm^{-1} exerts a large perturbation on absorption difference anisotropies (cf. the 7- and 21-pigment models discussed above), and it will certainly influence the steady-state LD and CD spectra as well. Realistic exciton models will clearly require explicit averaging over inhomogeneous diagonal energy distributions. The current disagreement between the assignments of BChl diagonal energies based on fits to absorption and CD spectra (Lu and Pearlstein, 1992) and absorption, LD, and singlet-triplet absorption difference spectra (Gülen, 1996) may stem in part from the sensitivity of anisotropic spectral properties to diagonal disorder in the FMO protein.

In separate anisotropy simulations, we considered the third scenario, where laser-prepared states exhibiting C_3 symmetry evolve into 7-pigment states before the probe pulse ~200 fs after excitation. The computed one- and two-color anisotropies were numerically small (typically $|r| < 0.1$ for the pump-probe wavelengths used) and did not resemble the ones observed. This comparison is unaffected by whether optical pump-probe coherence at early times masks fast (<100 fs) localization from 21- to 7-pigment states. Such coherence would not alter the initial state preparation (delocalized over 21 pigments) or its influence on the anisotropy at measurable times.

SUMMARY

Exciton calculations on symmetric and asymmetric FMO trimers, combined with absorption difference anisotropy measurements, suggest that the diagonal energy disorder in real samples at 19 K is sufficient to cause extensive localization in the laser-excited one-exciton states. Experimental anisotropies of FMO trimers from *Cb. tepidum* are inconsistent with 21-pigment exciton simulations based on a threefold-symmetric FMO protein. However, they qualitatively agree with a 7-pigment model that assumes that the laser-prepared states are localized within a subunit of the trimer. Differential diagonal energy shifts of 50 cm^{-1} between symmetry-related pigments in different subunits cause sharp localization in the stationary states. These shifts are commensurate with the ~95 cm^{-1} inhomogeneous linewidth of the lowest exciton levels. Experimental anisotropies (and by implication steady-state linear and circular dichroism) of FMO trimers likely arise from statistical averaging over widely contrasting values of these observables, in consequence of their sensitivity to diagonal energy disorder.

We thank Wenli Zhou and Robert Blankenship for supplying us with the FMO trimers from *Cb. tepidum*. We are indebted to Gerald Small for a seminal discussion.

The Ames Laboratory is operated for the U.S. Department of Energy by Iowa State University under contract W-7405-Eng-82. This work was supported by the Division of Chemical Sciences, Office of Basic Energy Sciences.

REFERENCES

Becker, M., V. Nagarajan, and W. W. Parson. 1991. Properties of the excited-singlet states of bacteriochlorophyll *a* and bacteriopheophytin *a* in polar solvents. *J. Am. Chem. Soc.* 113:6840–6848.

Blankenship, R. E., P. Cheng, T. P. Causgrove, D. C. Brune, S. H.-H. Wang, J.-U. Choh, and J. Wang. 1993. Redox regulation of energy transfer efficiency in antennas of green photosynthetic bacteria. *Photochem. Photobiol.* 57:103–107.

Blankenship, R. E., J. M. Olson, and M. Miller. 1995. Antenna complexes from green photosynthetic bacteria. *In* Anoxygenic Photosynthetic Bacteria. R. E. Blankenship, M. T. Madigan, and C. E. Bauer, editors. Kluwer Academic Publishers, Dordrecht, The Netherlands. 400–435.

Buck, D. R., S. Savikhin, and W. S. Struve. 1997. Ultrafast absorption difference spectra of the Fenna-Matthews-Olson protein at 19 K: experiment and simulations. *Biophys. J.* 72:24–36.

Chachisvilis, M., and V. Sundström. 1996. The tunnelling contributions to optical coherence in femtosecond pump-probe spectroscopy of the three level system. *J. Chem. Phys.* 104:5734–5744.

Daurat-Larroque, S. T., K. Brew, and R. E. Fenna. 1986. The complete amino acid sequence of a bacteriochlorophyll *a* protein from *Prosthecochloris aestuarii*. *J. Biol. Chem.* 261:3607–3615.

De Boer, S., and D. A. Wiersma. 1990. Dephasing-induced damping of superradiant emission in J-aggregates. *Chem. Phys. Lett.* 165:45–53.

Gülen, D. 1996. Interpretation of the excited-state structure of the Fenna-Matthews-Olson pigment protein complex of *Prosthecochloris aestuarii* based on the simultaneous simulation of the 4 K absorption, linear dichroism, and singlet-triplet absorption difference spectra: a possible excitonic explanation? *J. Phys. Chem.* 100:17683–17689.

Johnson, S. G., and G. J. Small. 1991. Excited state structure and energy transfer dynamics of the bacteriochlorophyll *a* antenna complex from *Prosthecochloris aestuarii*. *J. Phys. Chem.* 95:471–479.

Lu, X., and R. M. Pearlstein. 1993. Simulations of *Prosthecochloris* bacteriochlorophyll *a* - protein optical spectra improved by parametric computer search. *Photochem. Photobiol* 57:86–91.

Matthews, B. W., and R. E. Fenna. 1980. Structure of a green bacteriochlorophyll protein. *Acc. Chem. Res.* 13:309–317.

Olson, J. M. 1980a. Chlorophyll organization in green photosynthetic bacteria. *Biochim. Biophys. Acta.* 594:33–51.

Olson, J. M. 1980b. Bacteriochlorophyll *a* - proteins of two green photosynthetic bacteria. *Methods Enzymol.* 69:336–344.

Olson, J. M., B. Ke, and K. H. Thompson. 1976. Exciton interactions among chlorophyll molecules in bacteriochlorophyll *a* proteins and bacteriochlorophyll *a* reaction center complexes from green bacteria. *Biochim. Biophys. Acta.* 430:524–537.

Pearlstein, R. M. 1992. Theory of the optical spectra of the bacteriochlorophyll *a* antenna protein trimer from *Prosthecochloris aestuarii*. *Photosynth. Res.* 31:213–226.

Philipson, K. D., and K. Sauer. 1972. Exciton interaction in a bacteriochlorophyll protein from *Chloropseudomonas ethylica*: absorption and circular dichroism at 77 K. *Biochemistry.* 11:1880–1885.

Pullerits, T., and V. Sundström. 1996. Photosynthetic light-harvesting pigment-protein complexes: toward understanding how and why. *Acc. Chem. Res.* 29:381–389.

Reddy, N. R. S., R. Jankowiak, and G. J. Small. 1995. High-pressure hole-burning studies of the bacteriochlorophyll *a* antenna complex from *Chlorobium tepidum*. *J. Phys. Chem.* 99:16168–16178.

Savikhin, S. 1995. Shot-noise-limited detection of absorbance changes induced by subpicojoule laser pulses in optical pump-probe experiments. *Rev. Sci. Instrum.* 66:4470–4474.

Savikhin, S., and W. S. Struve. 1994. Ultrafast energy transfer in FMO trimers from the green bacterium *Chlorobium tepidum*. *Biochemistry.* 33:11200–11208.

Savikhin, S., and W. S. Struve. 1996. Low-temperature energy transfer in FMO trimers from the green photosynthetic bacterium *Chlorobium tepidum*. *Photosynth. Res.* 48:271–276.

Savikhin, S., W. Zhou, R. E. Blankenship, and W. S. Struve. 1994a. Femtosecond energy transfer and spectral equilibration in bacteriochlorophyll *a* - protein antenna trimers from the green bacterium *Chlorobium tepidum*. *Biophys. J.* 66:110–114.

Savikhin, S., Y. Zhu, S. Lin, R. E. Blankenship, and W. S. Struve. 1994b. Femtosecond spectroscopy of chlorosome antennas from the green photosynthetic bacterium *Chloroflexus aurantiacus*. *J. Phys. Chem.* 98: 10322–10334.

Sundström, V., and R. van Grondelle. 1995. Kinetics of excitation transfer, and trapping in purple bacteria. *In* Anoxygenic Photosynthetic Bacteria. R. E. Blankenship, M. T. Madigan, and C. E. Bauer, editors. Kluwer Academic Publishers, Dordrecht, The Netherlands. 349–372.

Tronrud, D. E., M. F. Schmid, and B. W. Matthews. 1986. Structure and x-ray amino acid sequence of a bacteriochlorophyll *a* protein from *Prosthecochloris aestuarii* refined at 1.9 Å resolution. *J. Mol. Biol.* 188:443–454.

Weiss, C. 1972. The pi electron structure and absorption spectra of chlorophylls in solution. *J. Mol. Spectrosc.* 44:37–80.

Zuber, H., and R. J. Cogdell. 1995. Purple bacterial antenna complexes. *In* Anoxygenic Photosynthetic Bacteria. R. E. Blankenship, M. T. Madigan, and C. E. Bauer, editors. Kluwer Academic Publishers, Dordrecht, The Netherlands. 315–348.